Quantification of root water uptake in soil using X-ray Computed Tomography and image based modelling.

Author list: Keith R. Daly[$§1], Saoirse R. Tracy[$2], Neil M. J. Crout[3], Stefan Mairhofer[4], Tony P. Pridmore[4], Sacha J. Mooney[3] and Tiina Roose[1]

Author affiliations:

[1] Bioengineering Sciences Research Group, Faculty of Engineering and Environment, University of Southampton, University Road, Southampton, SO17 1BJ, United Kingdom,

[2] School of Agriculture and Food Science, University College Dublin, Belfield Campus, Dublin 4, Ireland.

[3] School of Biosciences, University of Nottingham, Sutton Bonington Campus, Leicestershire, LE12 5RD, United Kingdom.

[4] School of Computer Science, University of Nottingham, Jubilee Campus, Nottingham, NG8 1BB, United Kingdom.

[$] These authors are joint lead authors

[§] Corresponding author: email: krd103@soton.ac.uk

1. Abstract

Spatially averaged models of root-soil interactions are often used to calculate plant water uptake. Using a combination of X-ray Computed Tomography (CT) and image based modelling we tested the accuracy of this spatial averaging by directly calculating plant water uptake for young wheat plants in two soil types. The root system was imaged using X-ray CT at 2, 4, 6, 8 and 12 days after transplanting. The roots were segmented using semi-automated root tracking for speed and reproducibility. The segmented geometries were converted to a mesh suitable for the numerical solution of Richards' equation. Richards' equation was parameterised using existing pore scale studies of soil hydraulic properties in the rhizosphere of wheat plants. Image based modelling allows the spatial distribution of water around the root to be visualised and the fluxes into the root to be calculated. By comparing the results obtained through image based modelling to spatially averaged models, the impact of root architecture and geometry in water uptake was quantified. We observed that the spatially averaged models performed well in comparison to the image based models with <2% difference in uptake. However, the spatial averaging loses important information regarding the spatial distribution of water near the root system.

Keywords: Matric potential; rhizosphere; root water uptake; soil pores; wheat; water release characteristic; X-ray Computed Tomography; image based homogenisation.

Abbreviations:

(CT) – Computed Tomography

Short title for page headings: Quantification of root water uptake in soil

2. Introduction

The fundamentals of plant water uptake, in particular the influence of the geometry of micro-scale root-soil interactions, are not fully understood. Further knowledge surrounding the mechanisms behind water flow in soil and into roots is crucial for modelling root water uptake. As plants grow they alter the soil immediately adjacent to the root creating a region known as the rhizosphere (Hiltner, 1904) through a combination of mechanical compression of the soil (Dexter, 1987; Whalley et al., 2013; Whalley et al., 2005), creation of biopores (Stirzaker et al., 1996) and exudation of chemical compounds such as mucilage (Czarnes et al., 2000) which, in turn, enhances microbial growth (Gregory, 2006). The role of the rhizosphere in terms of water retention and uptake has been the subject of a great number of studies . In dry conditions it is found that the rhizosphere is wetter than the surrounding soil, whilst in wet conditions the rhizosphere is drier than the surrounding soil (Carminati, 2012; Moradi et al., 2011). Other studies suggest rhizosphere soil may be wetter than bulk soil (Young, 1995) due to the formation of a coherent sheath of soil permeated by mucilage and root hairs, known as the rhizosheath (Gregory, 2006). Small quantities of water are released from the root to the rhizosheath at night while the root absorbs water from the rhizosheath during the day (Walker et al., 2003). The soil around a root and the processes that take place to form the rhizosphere soil clearly have a significant influence on root water uptake. However, currently we cannot mechanistically predict the role that root geometry plays in water uptake. This is due to the difficulties associated with imaging and quantifying roots, soil, and water simultaneously for growing root systems.

In order to improve understanding and provide a detailed description of water movement in and around the rhizosphere, research has generally focused on a combination of imaging and image based modelling studies (Daly et al., 2015). It is possible to use X-ray CT to quantify soil structure, water and air filled pore space (Rogasik et al., 1999) and, from the images generated, model partially saturated hydraulic conductivity in bulk soil (Tracy et al., 2015). Recently 3-dimensional (3D) segmented root architectures of faba bean (*Vicia faba* L.) have been used in a root-soil water movement model to determine the hydrodynamics of root water uptake in a split pot system (Koebernick et al., 2015). At the plant root scale, it is not computationally feasible to resolve the pore geometry in detail and averaged models for flow and transport are often used (Hornung, 1997; Keller, 1980; Richards, 1931). Formally, these models can be derived from the underlying pore scale models using mathematical techniques such as homogenisation (Cioranescu and Donato, 1999; Pavliotis and Stuart, 2008). Homogenisation methods are based around the idea that the behaviour of a system can be calculated by solving underlying equations on a representative region of soil. From a physical point of view, this method provides averaged equations and the means to derive the value of physical constants on which these equations depend based on the observed X-ray CT images. These methods are well suited to flow problems in soil and have been developed for single porosity materials (Hornung, 1997; Keller, 1980), double porosity materials (Arbogast and Lehr, 2006; Panfilov, 2000), porous media containing large separations in pore sizes (Arbogast and Lehr, 2006; Daly and Roose, 2014), and multi-fluid systems (Daly and Roose, 2015).

There are numerous models for root water uptake available in the literature, (see the reviews by Roose and Schnepf, (2008), Vereecken et al., (2016) and references therein). An early model by Landsberg and Fowkes (1978) considered water movement in a single root with the soil potential known a-priori. Rowse et al., (1978) modelled the spatial distribution of soil water as a function of depth and considered a spatially averaged uptake term to describe extraction of water by plant roots. Roose and Fowler (2004) were one of the first to consider the coupling of these two approaches, *i.e.*, calculating both soil moisture and water movement in the root. Their approach was based on a carefully derived uptake term averaged in the horizontal direction coupled to a model for root growth. Spatially explicit models for root water uptake are relatively recent and are based on 2D imaged or idealised architectures (Doussan et al., 2006). Such models have also been realised in three dimensions (Koebernick et al., 2015). In these models root water uptake is calculated through a sink term which effectively averages over a small volume, $0.5\times0.5\times0.25$ cm^3 in the case of Koebernick et al., (2015). There is a clear need to evaluate the effects of this sort of averaging and quantify how it affects models for root water uptake.

In this paper we address this question at the plant root scale. Our aim is to quantify the role that root geometry has on water uptake and how spatial averaging of root properties can affect the measured uptake. Throughout this paper we use the term 'root geometry' to refer to the complete root architecture rather than individual roots. We compare water uptake predicted by the spatially averaged model of Roose and Fowler, (2004), which is representative of averaged uptake models, and one which explicitly takes the root geometry into account. In order to facilitate the most direct comparison we parameterise the averaged model directly from the X-ray CT data through a single effective sink term. The equations are solved using finite element modelling to directly capture the influence of root geometry on uptake of water at the soil-root interface.

3. Materials and Methods

3.1. Sample preparation

Soil was obtained from The University of Nottingham experimental farm at Bunny, Nottinghamshire, UK (52.52° N, 1.07° W). The soils used in this study were a Eutric Cambisol (Newport series, loamy sand) and an Argillic Pelosol (Worcester series, clay loam). Particle size analysis for the two soils was: 83% sand, 13% clay, 4% silt for the Newport series and 36% sand, 33% clay, 31% silt for the Worcester series. Typical organic matter contents were 2.3% for the Newport series and 5.5% for the Worcester series (Mooney and Morris, 2008). Loose soil was collected from each site in sample bags, the soil was dried, sieved to <2 mm and packed into columns at a bulk density of 1.2 Mg m^{-3}. The columns were 80 mm high, had diameter of 50 mm and had mesh attached to the bottom to allow free drainage. The soil was mixed to distribute the different sized soil particles evenly before pouring it in small quantities into the columns. After compacting the soil in ten separate layers per column, the surface was lightly scarified to ensure homogeneous packing and hydraulic continuity within the column (Lewis and Sjostrom, 2010). The soil columns were saturated slowly by standing them in a tray of water to enable wetting from the base for 12 h. The columns were then allowed to drain freely for 48 h (Veihmeyer and Hendrickson, 1931), to replicate a soil moisture content close to a typical field capacity of a soil e.g. two days after a rainfall event. All columns were weighed and maintained at this weight throughout the experiment by adding the required volume of water daily to the top of the column to ensure soil moisture content remained near a notional field capacity. The columns were planted with a single wheat seed (*cv.* Zebedee) that had been pre-germinated on wet tissue paper for two days and grown for 12 days in a growth room with a 16 hr day at 24ºC and a 8 hr night at 18ºC with a humidity of 50%. As the soils were extracted from frequently fertilised agricultural fields and the experimental growth period was short, no additional nutrients were added to the columns. The samples were then imaged using X-ray CT at 0, 2, 4, 6, 8, and 12 days after transplanting (see section 3.2). Samples that had not been scanned, but set up identically, were also destructively analysed to determine any potential harmful effects on plant growth of the X-ray CT scanning. To ensure that the time taken for scanning did not impact on the plant growth, the samples were scanned during their night cycle. Also the plants that were not scanned were taken out of the growth room for the same amount of time as the pots that were scanned to ensure that any observable differences could be only attributed to scanning and not a result of the slight changes in environmental conditions.

At the end of the growth period the roots were washed from the soil and analysed using WinRHIZO™ 2002c scanning equipment and software to determine root volume and surface area, total root length and root diameter. Studies have shown that the X-ray dose received by the scanned samples had no discernible effect on root phenotypic traits (Zappala et al., 2013). This was confirmed by using WinRHIZO™ to scan plants which had undergone X-ray CT and control samples which had not.

3.2. X-ray Computed Tomography and image analysis

X-ray CT scanning was performed using a Phoenix Nanotom 180NF (GE Sensing & Inspection Technologies GmbH, Wunstorf, Germany). The scanner consisted of a 180 kV nanofocus X-ray tube fitted with a diamond transmission target and a 5-megapixel (2316 x 2316 pixels) flat panel detector (Hamamatsu Photonics KK, Shizuoka, Japan). The whole soil column was scanned at 0, 2, 4, 6, 8 and 12 days after transplanting. A maximum X-ray energy of 130 kV and 140 µA with a copper filter of 0.05 mm was used to scan each soil core. A total of 1200 projection images were acquired over a 360° rotation. The resulting isotropic voxel edge length was 30 μm and total scan time was 40 minutes per core. Two small aluminium and copper reference objects (< 1 mm^2) were attached to the side of the soil core to assist with image calibration and alignment during image analysis. Reconstruction of the projection images to produce 3D volumetric data sets was performed using the software datos|rec (GE Sensing & Inspection Technologies GmbH, Wunstorf, Germany).

The reconstructed X-ray CT volumes were visualised and quantified using VG StudioMAX® 2.2 (Volume Graphics GmbH, Heidelberg, Germany). Roots were segmented using a combination of the semi-automated root tracking software RooTrak (Mairhofer et al., 2012) followed by segmentation in VG StudioMAX® 2.2. Image stacks of the extracted volumes for each phase were exported and subsequently analysed.

3.3. Model preparation

In order to produce a smoothed geometry, from which computational meshes could be generated, several pre-processing steps were conducted. First the exported image stacks were down sampled to reduce the resolution of the scans by a factor of 4. This process combines pixels, smoothing out small features and noise present in the segmented images. Finally, a three pixel median filter was applied to the data to create smooth representation of the root segmented from the surrounding soil. To remove any artefacts from the segmented image the root geometry was skeletonized and a connected volume analysis was used to remove any sections of root which did not connect to the top slice. The skeletonized root geometry was then dilated to the average root radius to provide a geometry on which the simulations could be performed. This smoothing process has the benefit of removing small artefacts which could affect mesh generation. However, it will also alter the root geometry, in particular the surface area. This variation, in addition to the finite resolution of the X-ray CT imaging and segmentation procedures, means that it is not possible to determine absolute water uptake with 100% accuracy, (Tracy et al., 2015). These sources of error will be absolute errors and will not affect relative water uptake across different time points or simulation methods in this study.

A computational mesh was generated based on the root geometries using Simpleware 7.0, a commercial software package used to generated finite element and surface meshes from the imaged data. The mesh generated was designed for Comsol Multiphysics and was created using the FE-FREE algorithm to allow Simpleware the maximum control over the elements whilst minimizing the memory usage of the mesh. The meshes consisted of *circa.* 1,500,000 elements and contained segmented boundaries which described the root surface, the soil-air interface and the pot surface.

3.4. Root water uptake

3.4.1. A priori estimates

To determine the appropriate conditions to apply on the root surface we first consider the movement of water within the root. Based on a cylindrical root approximation it has been shown that root water uptake falls into one of three distinct regimes (Roose and Fowler, 2004): large thick roots, medium roots or small thin roots. These regimes are described by a different boundary condition on the root surface and are dependent on the geometrical properties of the root itself through the dimensionless parameter

$$\kappa^2 = \frac{2\pi a L^2 k_r}{k_z}, \tag{1}$$

which quantifies the importance of the radial water transport with respect to axial water transport through the root. Here L is the root length, a is the root radius, k_r is the radial hydraulic conductivity of the root and k_z is the axial hydraulic conductivity of the root. For the cases of small thin roots, $\kappa^2 \gg 1$ and large thick roots, $\kappa^2 \ll 1$, the root surface boundary condition can be simplified.

We parameterise our model based on a typical X-ray CT scan of a 12 day old plant and used $k_r = 1.3 \times 10^{-13}\text{m s}^{-1}\text{Pa}$ (Jones et al., 1983), $k_z = 2 \times 10^{-16}\text{m}^4\text{ s}^{-1}\text{ Pa}^{-1}$ (Payvandi et al., 2014; Percival, 1921). We find, for a typical root radius of 0.39 mm (13 voxels) and root length of 60 mm (2000 voxels), $\kappa^2 = 0.0107$ corresponding to large thick roots with an internal pressure

$$p_r = p_0 + \rho g z, \tag{2}$$

where p_0 is the pressure applied by the plant with $p_0 = -1$ MPa during the day, (Passioura, 1983), and $p_0 = 0$ MPa at night, ρ is the density of water and g the acceleration due to gravity (Roose and Fowler, 2004). These approximations are valid for cylindrical roots aligned along the z-axis. However, the approximation $\kappa^2 \ll 1$ remains valid as long as the roots do not deviate significantly from a cylindrical geometry. Any deviations in the root geometry from a cylindrical shape will induce an error in the approximation. We can approximate the error induced by this by calculating the size of the z dependent term in equation (2). In this case $|p_0| = 1$ MPa and $\rho g L \approx 500$ Pa, where $L \approx 50$ mm is the root length we have $p_0 \gg \rho g L$, so the variation in root pressure across the geometry will be small and we can approximate equation (2) as

$$p_r = p_0. \tag{3}$$

Hence, there will have to be significant deviation of the root from a cylindrical geometry for there to be any noticeable effect on the root pressure.

3.4.2. **Richards' equation**

To model the flow of water around the root we use Richards' equation for partially saturated flow (Richards, 1931). This equation is parameterized by the water release curve and the saturation dependent hydraulic conductivity, which we will characterize using the well-known Van-Genuchten Mualem model (Mualem, 1976; Van Genuchten, 1980). For compactness we will assume the same notation as used in (Roose and Fowler, 2004) and will present only the final equations and main assumptions used in this manuscript.

We assume that the soil geometry is homogeneous. Hence, we are able to describe the water content in terms of relative saturation, which, assuming conservation of mass can be written as

$$\phi \frac{\partial S}{\partial t} + \boldsymbol{\nabla} \cdot \boldsymbol{u} = 0 \tag{4}$$

where S is the average relative water saturation defined as the total volume of water per unit pore space, ϕ is the porosity of the soil and $\boldsymbol{u}$ is the water velocity. In terms of saturation the fluid flux can be written as

$$\boldsymbol{u} = -[D_0 D(S)\boldsymbol{\nabla} S - K_s K(S)\hat{\boldsymbol{e}}_z] \tag{5}$$

where

$$K(S) = S^{1/2}\left[1 - \left(1 - S^{\frac{1}{m}}\right)^m\right]^2, \tag{6}$$

$$D(S) = S^{\frac{1}{2}-\frac{1}{m}}\left[\left(1 - S^{\frac{1}{m}}\right)^m + \left(1 - S^{\frac{1}{m}}\right)^{-m} - 2\right], \tag{7}$$

$D_0 = \frac{p_c k_s}{\mu}\left(\frac{1-m}{m}\right)$, $K_s = \frac{\rho g k_s}{\mu}$, ρ and μ are the density and viscosity of water respectively, m is the Van-Genuchten parameter (Van Genuchten, 1980), g is the acceleration due to gravity, p_c is a characteristic suction pressure, k_s is the saturated water permeability and $\hat{\boldsymbol{e}}_z$ is a unit vector in the direction of gravity. The mathematical symbols, their meaning and units are summarised in Table 1.

The root exerts a suction pressure given by equation (3) on the soil. This induces a pressure drop across the soil and acts to draw water into the root. This pressure is related to the suction through the Van-Genuchten equation (Van Genuchten, 1980) which, on the surface of the root, can be written as

$$-\hat{\boldsymbol{n}} \cdot [D_0 D(S)\boldsymbol{\nabla} S - K_s K(S)\hat{\boldsymbol{e}}_z] = k_r(p_c f(S) - p_0), \tag{8}$$

where $\hat{\boldsymbol{n}}$ is the unit normal to the root surface and

$$f(S) = \left(S^{-\frac{1}{m}} - 1\right)^{1-m}. \tag{9}$$

The remaining external boundaries are assumed to be impermeable to fluid, hence we write $\hat{\boldsymbol{n}} \cdot \boldsymbol{u} = 0$ on the outer pot boundary. The boundary condition at the bottom is $\hat{\boldsymbol{n}} \cdot \boldsymbol{u} = K(S)$, i.e., the only water flux at the bottom of the pot is due to gravity and at the top $\hat{\boldsymbol{n}} \cdot \boldsymbol{u} = q_s$ where $q_s(t)$ is the flux of water into the soil. We use, as an initial condition, $S = 0.5$ corresponding to a plant which has been recently watered and consider the case $q_s(t) = 0$.

The parameters used in these equations are taken from the literature and previous studies on soil water imaging. Specifically we use $k_r = 1.3 \times 10^{-13} \mathrm{m\,s^{-1}Pa^{-1}}$ (Jones et al., 1983), $k_z = 2 \times 10^{-16} \mathrm{m^4\,s^{-1}\,Pa^{-1}}$ (Payvandi et al., 2014; Percival, 1921). The soil water diffusivity, D_0, is taken directly from the literature and is set to $D_0 = 4.37 \times 10^{-6}\ \mathrm{m^2 s^{-1}}$ (Van Genuchten, 1980). The hydraulic conductivity, K_s, and the Van-Genuchten parameter, m, are taken from Daly et al. (2015) for the two different soil types. Specifically we use m =0.415 and $K_s = 1.09 \times 10^{-5}\ \mathrm{m\,s^{-1}}$ for the clay loam and $m = 0.397$ and $K_s = 2.46 \times 10^{-5}\ \mathrm{m\,s^{-1}}$ for the loamy sand soil.

The equations described above are implemented directly on the numerical meshes generated by Simpleware. Water uptake is simulated for a period of one day to calculate uptake over a single day-night cycle which consists of a 16 hour day and 8 hour night corresponding to the growth conditions. At night water uptake is assumed to be zero and evaporation is assumed to be zero throughout the simulation. The equations were solved using Comsol Multiphysics and are implemented as a general form partial differential equation. The simulations were run on a single 16 processor node of the Iridis 4 supercomputing cluster at the University of Southampton to calculate the water profile in the soil and root water uptake. Resource usage varied dependent on the complexity of the root geometry, the most expensive simulations used ≈ 90 Gb of memory and ran in under 60 hours.

3.4.3. Comparison with spatially averaged model

In order to quantify the effects of including the root architecture explicitly we compare our results to the averaged model developed in Roose and Fowler (2004). This averaged model is based on the observation that, for sufficiently small inter-root spacing, any saturation gradients in the horizontal direction will equilibrate sufficiently quickly that variations in this direction may be neglected. The averaged model is derived by assuming that the uptake properties of the root system are equal across the whole root surface. This does not mean that the uptake across the root is equal. Rather, it is dependent on the soil water pressure which may vary with depth. Hence, the one dimensional equation for root water uptake is given by

$$\phi \frac{\partial S}{\partial t} + \boldsymbol{\nabla} \cdot [D_0 D(S) \boldsymbol{\nabla} S - K_s K(S) \hat{\boldsymbol{e}}_z] = A_{eff} k_r (p_c f(S) - p_0), \tag{10}$$

where $A_{eff} = \frac{A_r}{L_r A_p}$, A_r is the root surface area, A_p is the cross sectional area of the pot and L_r is the root length. For direct comparison with the image based method these equations are solved in Comsol Multiphysics using the same implementation method as described above. In order to compare the two methods we define the difference in cumulative uptake as

$$e = \frac{2(I_A - I_I)}{(I_I + I_A)} \tag{11}$$

where I_A and I_I are the total uptake for the averaged model and the image based model respectively.

3.4.4. Statistical Analysis

The results obtained experimentally were analysed by general analysis of variance (ANOVA) containing soil type, time period and all possible interactions as explanatory variables using Genstat 15.1 (VSN International, UK). The probability of significance P, with a threshold value of ($P<0.05$), corresponding to a 95% confidence limit, was calculated and is used as a measure of significance of results obtained.

4. Results & Discussion

4.1. Soil pore geometry

No significant changes in soil volume from the imaging method were recorded across the experiment, confirming structural changes were due to alterations in the pore size distribution (Figure 1). Throughout the 12 days the average volume of air, imaged in the form of macropores, remained approximately constant in the loamy sand soil (Figure 1). Whilst there was large variation within treatment from day 2 until day 8, the average volume of imaged air filled pores was greater in the loamy sand soil than the clay soil ($P<0.01$). However, at day 12 this trend switched, so that the average air filled pore volume in a clay sample was 4268 mm^3 compared to just 3130 mm^3 in the loamy sand soil. From a visual inspection of the X-ray CT images this increase in air filled pore volume at day 12, after the samples have undergone several wetting and drying cycles, is attributed to crack formation in the clay soil due to its swelling and shrinking properties (see supplementary figures 1 and 2 for greyscale images) and is potentially linked to soil drying through root water uptake.

4.2. **Root system architecture**

The scanned root architectures for plants grown in the loamy sand and clay loam are shown in Figure 2 and Figure 3 respectively. No significant differences in root measurements were found between samples that had undergone X-ray CT scanning and those that had not ($P>0.05$), suggesting no harmful effects of X-ray dose on the plants (see supplementary table S1 for details). Root volumes as quantified by WinRHIZO™ were greater for plants grown in clay soil than for those grown in loamy sand soil ($P<0.05$). However, no significant differences were observed in root volume measured using X-ray CT. It would not be useful to draw comparisons between root measurements obtained via destructive root sampling (WinRHIZO™) and the non-destructive X-ray CT scanning due to the inherent differences in the techniques (e.g. 2D *vs.* 3D, in soil and without soil etc.), (Tracy et al., 2012). Using X-ray CT we observed a significant difference (710 mm^2 *vs.* 455 mm^2; $P<0.05$) in root surface area for plants grown in a clay loam compared to the loamy sand soil (Figure 1). Based on the CT images the majority of growth took place in the first four days. Ideally, a higher frequency of scans at this point in the root development would have facilitated a clearer picture of root growth. However, due to the cost and time taken to scan and process this data we were not able to obtain additional scans in the first four days.

We did not observe fine lateral roots in the CT scans due to the resolution. However, it is known that the axial conductivity of the xylem scales with the fourth power of the root radius

(Payvandi et al., 2014; Sevanto, 2014; Thompson and Holbrook, 2003). As a result, water movement in fine laterals will be much slower than the primary roots. Hence, it has been suggested that fine laterals are less important in terms of water uptake (Roose and Fowler, 2004). The increase in measured root mass comes directly from an increase in the primary roots. Over the course of the experiments the roots did not become pot bound; this was evidenced through measuring maximum width and depth of the root system. The average width at day 12 was 39 mm, which was less than the pot diameter of 50 mm, and the average depth at day 12 was 47 mm, which was less than the pot depth of 80 mm.

4.3. **Root water uptake**

Over the 12 day experiment the watering regime remained constant. However, at day 8 a reduction in water content was measured via imaging (Figure 1; $P<0.001$). It is possible that, at day 8, the plant stopped being reliant on seed reserves and began capturing resources from the soil (Kennedy et al., 2004). However, we observed that this reduction in water content disappeared at day 12. It is possible that a temporary increase in the rate of water uptake occurs at this time, possibly related to the formation of lateral roots. However there is not sufficient evidence to confirm this and the dip may simply be a result of imaging/segmentation errors or minor differences in the watering regime. Hence, further investigation is needed to quantify these effects.

To quantify the regions from which water has been taken we consider the numerical simulations. We visualised the water distribution within the soil by calculating regions of equal saturation. As we are considering a 3D dataset the regions of equal saturation (S) will show up as surfaces. We visualised these surfaces at different times after watering in Figure 4, Figure 5 and the supplementary material. These surfaces are plotted for a single plant at 2, 4, 6, 8 and 12 days after planting for three different times within the uptake cycle. A clear depletion in water content was observed over the course of a day.

In addition, the simulations show that water content is lower near the roots generating a net flux of water towards the plant. This lower moisture content in the region immediately adjacent to the root is in line with the observation that water content in the rhizosphere is lower than the moisture content far from the root (Carminati, 2012; Moradi et al., 2011). However, we note that in these simulations we do not explicitly treat the soil adjacent to the root differently to the soil far from the root. This effect is more pronounced in the clay soil (Figure 5), than the loamy sand (Figure 4) and can be seen by the density of the equal saturation surfaces in the figures.

In order to quantify the uptake rate and total uptake of the roots over the course of the day-night, we calculated the flux and cumulative uptake, averaged over all replicates, for the clay loam and loamy sand soils (Figure 6 and supplementary material). The largest change in water uptake, based on simulation, occurs in the first four days of root development. We note that, due to the watering regime, these changes will not be echoed in the volumetric water content, Figure 1. Whilst there are still changes after this point, these are not as pronounced. We do not observe any dip in water uptake at day 8. This suggests that the observed decrease in volumetric water content is due to processes which are not being measured. Whilst it is tempting to attribute this difference to the presence of fine laterals, this does not explain the disappearance of this dip at day 12. In addition, any fine laterals, which are not observed in the X-ray CT imaging, will be significantly smaller than the primary roots observed. Therefore, their conductivity, and contribution to uptake, would be significantly smaller than that of the primary roots.

In order to quantify how the details of the root geometry affected water uptake, we compared the uptake predicted using these models to water uptake predicted by the simplified water uptake model developed by Roose and Fowler (2004). We consider water uptake over a 24 hour period. At the start of the simulation the water content is assumed constant over the root system with saturation S=0.5 throughout. This is comparable to the growth conditions in the columns which were rewatered to a known weight on a daily basis. The water content would then decrease due to a combination of water uptake and loss via drainage or evaporation over the 24 hour period. To facilitate the most direct comparison of the two methods we have used the root surface area extracted from the X-ray CT data to parameterise the model. This means that we are directly comparing how the geometrical properties of the root systems affect uptake and flux. The averaged and image based models agree well in terms of total uptake, Figure 6 and Figure 7. The difference in cumulative uptake defined in equation (11) is less than 2%, Figure 7.

In general, the imaged geometry predicts a smaller uptake than the averaged geometry. The largest difference is observed for the older plants, $\approx$ 1.25% for the plants grown in the sandy loam and $\approx$ 1% for the plants grown in clay loam. The difference is even smaller for the younger plants <1% for both soil types. To put this difference in context, the error for Neutron Magnetic Resonance imaging (NMRi) of water uptake is approximately 7% (Scheenen et al,. 2000). However, differences in soil pore water measurement between

Neutron probes and Time Domain Reflectometry can be as high as 12% (Smethurst et al,. 2006). There is also a wealth of information that cannot be investigated using the averaged models. In particular the local distribution of water around the root cannot be investigated by the averaged models. This means that any effect of soil inhomogeneity in the rhizosphere or crack formation, due to soil shrinkage and swelling, will be neglected. Hence, the use of averaged models is reasonable if the quantity of interest is simply the absolute uptake by the root system.

Image based modelling allows water uptake by plants to be calculated using observed root geometries and, in this study, provides comparable results to the averaged models. However, there are sources of error present in image based modelling which need to be considered carefully when interpreting these results. Firstly, the outputs of the uptake model are, at best, only as accurate as the imaging and segmentation procedures. As it is only possible to model what is observed, the segmented root system does not represent the full root system as fine lateral roots and root hairs will not be captured at the resolution of these scans. Hence, the contribution of these features of the root geometry to plant water uptake will not be captured. However, as the transport of water by plant roots scales with the fourth power of the root radius, we would expect that any sub resolution fine laterals would be insignificant. To quantify this we consider the uptake of roots at the limit of resolution. The roots which we do consider fall into the category of large thick roots, equation (1). Hence, their uptake is limited by the availability of water to the root. For the case of fine laterals of radius 30 μm we find $\kappa^2 = 12.6$, where we have scaled k_z to take into account the reduced root radius. This corresponds to small thin roots which have been shown, (Roose and Fowler, 2004), to only take up water in a region of length $L_u \propto 1/\kappa$ near to the base of the roots. Hence, the only contribution to uptake from laterals at the limit of resolution will be a small increase in uptake where they join the primary roots. Whilst it is not possible to precisely quantify this uptake, it is expected to be small compared to the relative errors of imaging, segmentation and meshing. Secondly, whilst every care has been taken to segment the roots in a reproducible and robust way, and every effort taken to minimise minor differences in signal-to-noise ratio between scans, no segmentation procedure is perfect. Finally, the assumptions used in this model such as soil homogeneity, uniform initial conditions and stationary root architecture are not necessarily realistic and will introduce errors into the results. Some of these limitations could be overcome using higher resolution X-ray CT imaging, but the trade-off between sample diameter and achievable resolution would remain, or by adapting the models to consider growing root architectures through interpolation (Daly et al., 2016) or repeated imaging (Koebernick et al., 2015).

Conclusions

In this paper we have shown that, for pots of 50 mm diameter, differences in plant water uptake can be observed between a spatially averaged model and an image based model. These differences can be quantified both in terms of uptake rate and cumulative uptake. The difference between the averaged and image based models was less than 2% for all cases considered, this is less than typical experimental error in plant water uptake measurements. The averaging methods were not able to resolve the soil moisture profile in three dimensions meaning that they would be unable to truly capture heterogeneity in the rhizosphere. Hence, whilst averaging is a useful method for quickly estimating water uptake, there is significant information lost which may be important in terms of understanding rhizosphere function.

There are several assumptions in the image based models and there is room for improvement. In principle the numerical modelling in this paper could be extended to older plants with much larger root systems and could include root growth through an effective growth rate into the model, a method which has been used to study nutrient uptake by root hairs (Daly et al., 2016). However, despite the assumptions present, non-destructive imaging combined with image based modelling remains a powerful tool to not only visualise soil geometry but to quantify the effects of the observable root architecture on plant water uptake.

5. Acknowledgements

The authors acknowledge the use of the IRIDIS High Performance Computing Facility, and associated support services at the University of Southampton, in the completion of this work. This project was funded by BBSRC BB/J000868/1, a collaborative project between the Universities of Southampton and Nottingham, PI and overall lead TR. KRD and TR are also funded by ERC consolidation grant 646809DIMR.

Data Accessibility

All reconstructed scan data will be available on request by emailing microct@nottingham.ac.uk. For simulation results please email krd103@soton.ac.uk.

6. References

Arbogast, T. and Lehr, H. L. (2006). Homogenization of a Darcy–Stokes system modeling vuggy porous media. *Computational Geosciences* **10**, 291-302.

Carminati, A. (2012). A model of root water uptake coupled with rhizosphere dynamics. *Vadose Zone Journal* **11**(3).

Cioranescu, D. and Donato, P. (1999). An introduction to homogenization: Oxford University Press Oxford.

Czarnes, S., Hallett, P. D., Bengough, A. G. and Young, I. M. (2000). Root- and microbial-derived mucilages affect soil structure and water transport. *European Journal of Soil Science* **51**, 435-443.

Daly, K. R., Keyes, S. D., Masum, S. and Roose, T. (2016). Image-based modelling of nutrient movement in and around the rhizosphere. *Journal of experimental botany* **67**, 1059-1070.

Daly, K. R., Mooney, S., Bennett, M., Crout, N., Roose, T. and Tracy, S. (2015). Assessing the influence of the rhizosphere on soil hydraulic properties using X-ray Computed Tomography and numerical modelling. *Journal of experimental botany* **66**, 2305-2314.

Daly, K. R. and Roose, T. (2014). Multiscale modelling of hydraulic conductivity in vuggy porous media. *Proceedings of the Royal Society A: Mathematical, Physical and Engineering Science* **470**(2162), 20130383.

Daly, K. R. and Roose, T. (2015). Homogenization of two fluid flow in porous media **471**(2176) 20140564.

Dexter, A. (1987). Compression of soil around roots. *Plant and Soil* **97**, 401-406.

Doussan, C., Pierret, A., Garrigues, E. and Pagès, L. (2006). Water uptake by plant roots: II–modelling of water transfer in the soil root-system with explicit account of flow within the root system–comparison with experiments. *Plant and Soil* **283**, 99-117.

Downie, H. F., Adu, M. O., Schmidt, S., Otten, W., Dupuy, L. X., White, P. J. and Valentine, T. A. (2014). Challenges and opportunities for quantifying roots and rhizosphere interactions through imaging and image analysis. *Plant Cell Environ **38**(7) 1213-1232*.

Gregory, P. (2006). Roots, rhizosphere and soil: the route to a better understanding of soil science? *European Journal of Soil Science* **57**, 2-12.

Hiltner, L. (1904). Über neuere Erfahrungen und Probleme auf dem Gebiete der Bodenbakteriologie unter besonderer Berücksichtigung der Gründüngung und Brache. *Arbeiten der Deutschen Landwirtschaftlichen Gesellschaft* **98**, 59-78.

Hornung, U. (1997). Homogenization and porous media: Springer.

Jones, H., Tomos, A. D., Leigh, R. A. and Jones, R. G. W. (1983). Water-relation parameters of epidermal and cortical cells in the primary root ofTriticum aestivum L. *Planta* **158**, 230-236.

Keller, J. B. (1980). Darcy's law for flow in porous media and the two-space method. In *Nonlinear partial differential equations in engineering and applied science (Proc. Conf., Univ. Rhode Island, Kingston, RI, 1979)*, vol. 54, pp. 429-443: Dekker New York.

Kennedy, P., Hausmann, N., Wenk, E. and Dawson, T. (2004). The importance of seed reserves for seedling performance: an integrated approach using morphological, physiological, and stable isotope techniques. *Oecologia* **141**, 547-554.

Koebernick, N., Huber, K., Kerkhofs, E., Vanderborght, J., Javaux, M., Vereecken, H. and Vetterlein, D. (2015). Unraveling the hydrodynamics of split root water uptake experiments using CT scanned root architectures and three dimensional flow simulations. *Frontiers in plant science* **6**, 370.

Landsberg, J. and Fowkes, N. (1978). Water movement through plant roots. *Annals of Botany* **42**, 493-508.

Lewis, J. and Sjostrom, J. (2010). Optimizing the experimental design of soil columns in saturated and unsaturated transport experiments. *Journal of Contaminant Hydrology* **115**, 1-13.

Mairhofer, S., Zappala, S., Tracy, S. R., Sturrock, C., Bennett, M., Mooney, S. J. and Pridmore, T. (2012). RooTrak: Automated Recovery of Three-Dimensional Plant Root

Architecture in Soil from X-Ray Microcomputed Tomography Images Using Visual Tracking. *Plant Physiology* **158**, 561-569.

Mooney, S. J. and Morris, C. (2008). A morphological approach to understanding preferential flow using image analysis with dye tracers and X-ray Computed Tomography. *CATENA* **73**, 204-211.

Mooney, S. J., Pridmore, T. P., Helliwell, J. and Bennett, M. J. (2012). Developing X-ray Computed Tomography to non-invasively image 3-D root systems architecture in soil. *Plant and Soil* **352**, 1-22.

Moradi, A. B., Carminati, A., Vetterlein, D., Vontobel, P., Lehmann, E., Weller, U., Hopmans, J. W., Vogel, H. J. and Oswald, S. E. (2011). Three-dimensional visualization and quantification of water content in the rhizosphere. *New Phytologist* **192**, 653-663.

Mualem, Y. (1976). A new model for predicting the hydraulic conductivity of unsaturated porous media. *Water Resources Research* **12**, 513-522.

Panfilov, M. (2000). Macroscale models of flow through highly heterogeneous porous media: Springer.

Passioura, J. (1983). Roots and drought resistance. *Agricultural water management* **7**, 265-280.

Pavliotis, G. and Stuart, A. (2008). Multiscale methods: averaging and homogenization: Springer Science & Business Media.

Payvandi, S., Daly, K. R., Jones, D., Talboys, P., Zygalakis, K. and Roose, T. (2014). A mathematical model of water and nutrient transport in xylem vessels of a wheat plant. *Bulletin of mathematical biology* **76**, 566-596.

Percival, J. (1921). The wheat plant: a monograph No. SB4191. W5 P4).

Richards, L. A. (1931). Capillary conduction of liquids through porous mediums. *Journal of Applied Physics* **1**, 318-333.

Rogasik, H., Crawford, J. W., Wendroth, O., Young, I. M., Joschko, M. and Ritz, K. (1999). Discrimination of soil phases by dual energy x-ray tomography. *Soil Science Society of America Journal* **63**, 741-751.

Roose, T. and Fowler, A. (2004). A model for water uptake by plant roots. *Journal of theoretical biology* **228**, 155-171.

Roose, T. and Schnepf, A. (2008). Mathematical models of plant–soil interaction. *Philosophical Transactions of the Royal Society A: Mathematical, Physical and Engineering Sciences* **366**, 4597-4611.

Rowse, H., Stone, D. and Gerwitz, A. (1978). Simulation of the water distribution in soil. *Plant and Soil* **49**, 533-550.

Sevanto, S. (2014). Phloem transport and drought. *Journal of experimental botany*, **65**(7) 1751-1759.

Scheenen, T. W. J., D. Van Dusschoten, P. A. De Jager, and H. Van As. "Quantification of water transport in plants with NMR imaging." *Journal of Experimental Botany* 51, no. 351 (2000): 1751-1759.

Smethurst, J.A., Clarke, D. and Powrie, W. (2006). Seasonal changes in pore water pressure in a grass covered cut slope in London Clay. Géotechnique, 56(8), 523-537.

Stirzaker, R. J., Passioura, J. B. and Wilms, Y. (1996). Soil structure and plant growth: Impact of bulk density and biopores. *Plant and Soil* **185**, 151-162.

Thompson, M. and Holbrook, N. (2003). Scaling phloem transport: water potential equilibrium and osmoregulatory flow. *Plant Cell Environ* **26**, 1561-1577.

Tracy, S. R., Daly, K. R., Sturrock, C. J., Crout, N. M. J., Mooney, S. J. and Roose, T. (2015). Three dimensional quantification of soil hydraulic properties using X-ray Computed Tomography and image based modelling *Water Resources Research **51**(2) 1006-1022*.

Tracy S.R., Black C.R., Roberts J.A., Sturrock C., Mairhofer S., Craigon J., Mooney S.J. (2012). Quantifying the impact of soil compaction on root system architecture in tomato (*Solanum lycopersicum* L.) by X-ray micro- Computed Tomography (CT). *Annals of Botany*. **110**, 511-519.

Van Genuchten, M. T. (1980). A closed-form equation for predicting the hydraulic conductivity of unsaturated soils. *Soil science society of America journal* **44**, 892-898.

Veihmeyer, F. and Hendrickson, A. (1931). The moisture equivalent as a measure of the field capacity of soils. *Soil Science* **32**, 181-194.

Vereecken, H., Schnepf, A., Hopmans, J.W., Javaux, M., Or, D., Roose, T., …, Young, I.M. (2016) Modeling soil processes: key challenges and new perspectives. *Vadose Zone Journal* **15**(5).

Walker, T. S., Bais, H. P., Grotewold, E. and Vivanco, J. M. (2003). Root exudation and rhizosphere biology. *Plant Physiology* **132**, 44-51.

Whalley, W., Ober, E. and Jenkins, M. (2013). Measurement of the matric potential of soil water in the rhizosphere. *Journal of experimental botany* **64**, 3951-3963.

Whalley, W. R., Riseley, B., Leeds-Harrison, P. B., Bird, N. R., Leech, P. K. and Adderley, W. P. (2005). Structural differences between bulk and rhizosphere soil. *European Journal of Soil Science* **56**, 353-360.

Young, I. M. (1995). Variation in moisture contents between bulk soil and the rhizosheath of wheat (Triticum-aestivum L cv Wembley). . *New Phytologist* **130**, 135-139.

Zappala, S., Helliwell, J. R., Tracy, S. R., Mairhofer, S., Sturrock, C. J., Pridmore, T., Bennett, M. and Mooney, S. J. (2013). Effects of X-ray dose on rhizosphere studies using X-ray computed tomography. *PloS one* **8**, E67250.

Figures

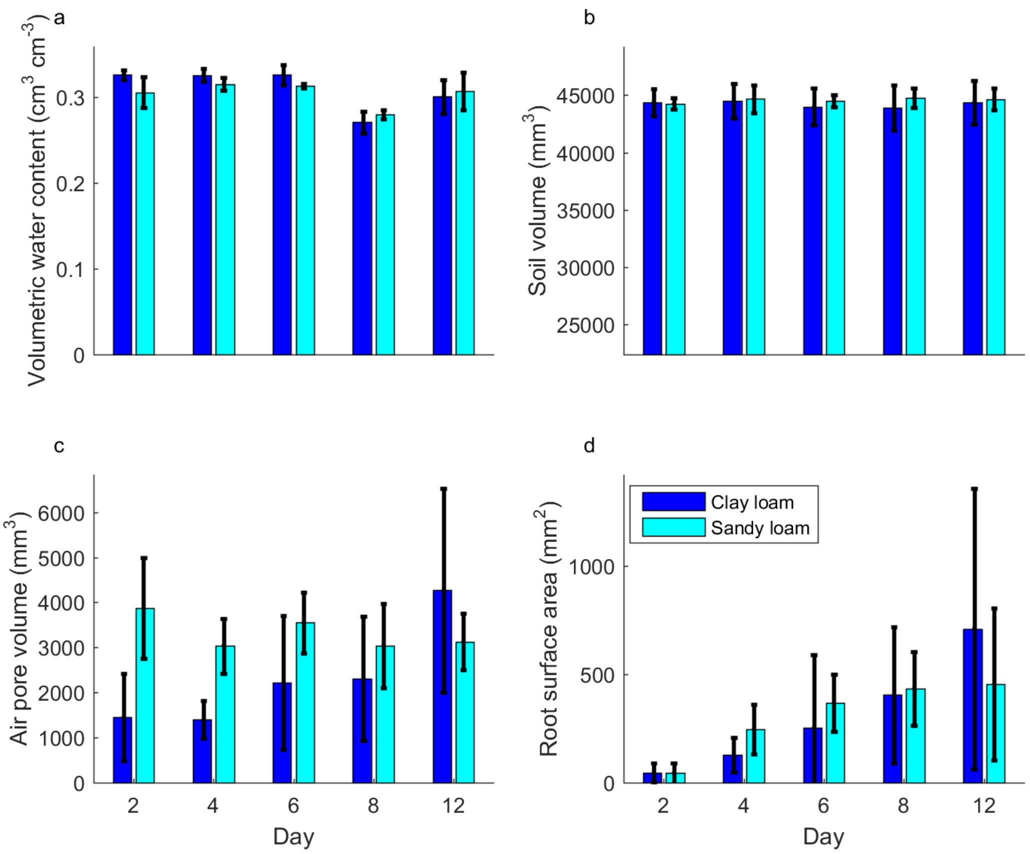

Figure 1 Imaged data for (a) volumetric water content, (b) soil volume, (c) air volume, and (d) root surface area.

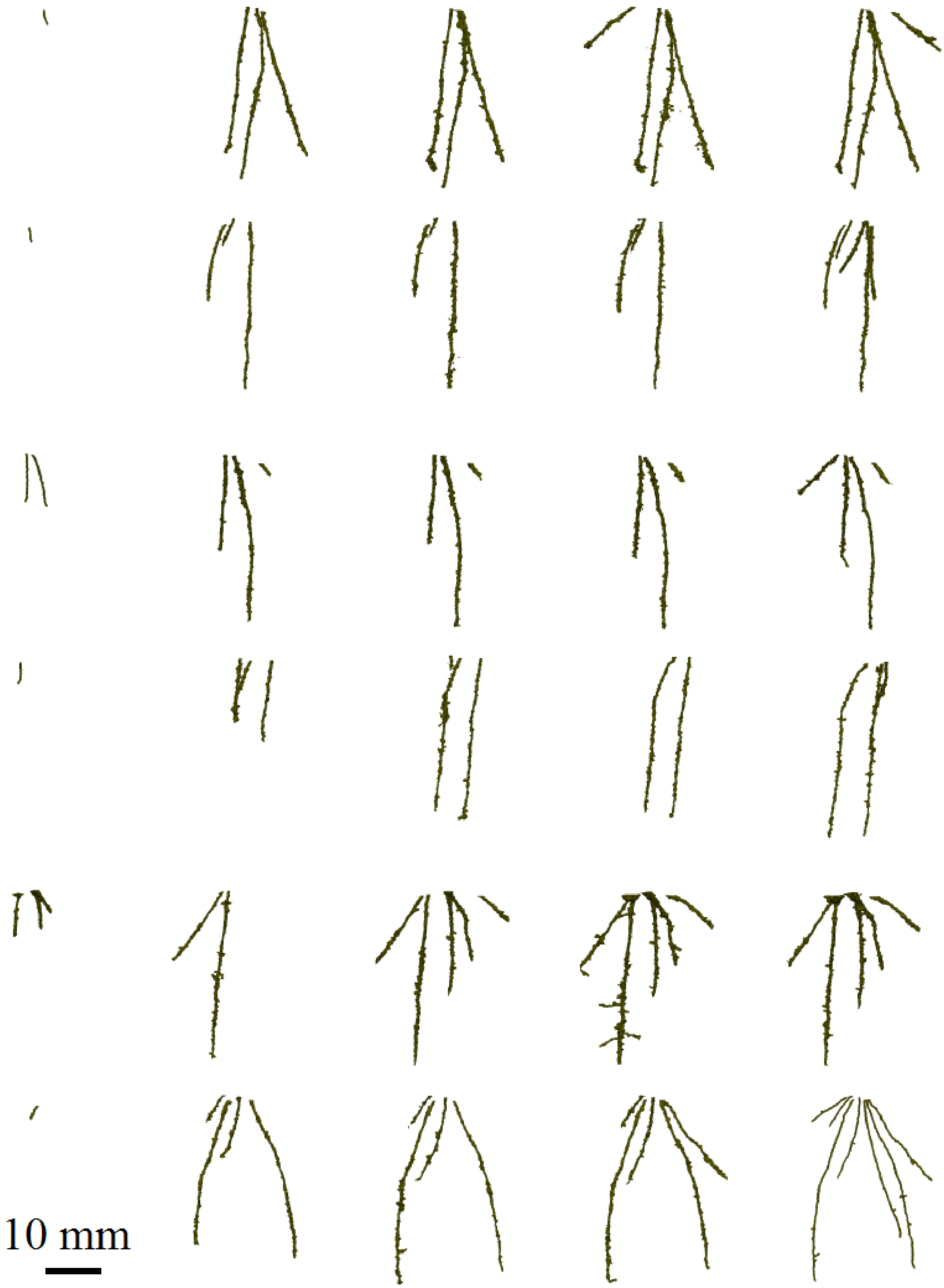

Figure 2: Root architectures for roots grown in loamy sand soil. Each row is a different sample. Columns correspond to Day 2, Day 4, Day 6, Day 8, Day 12. Scale bar is 10 mm.

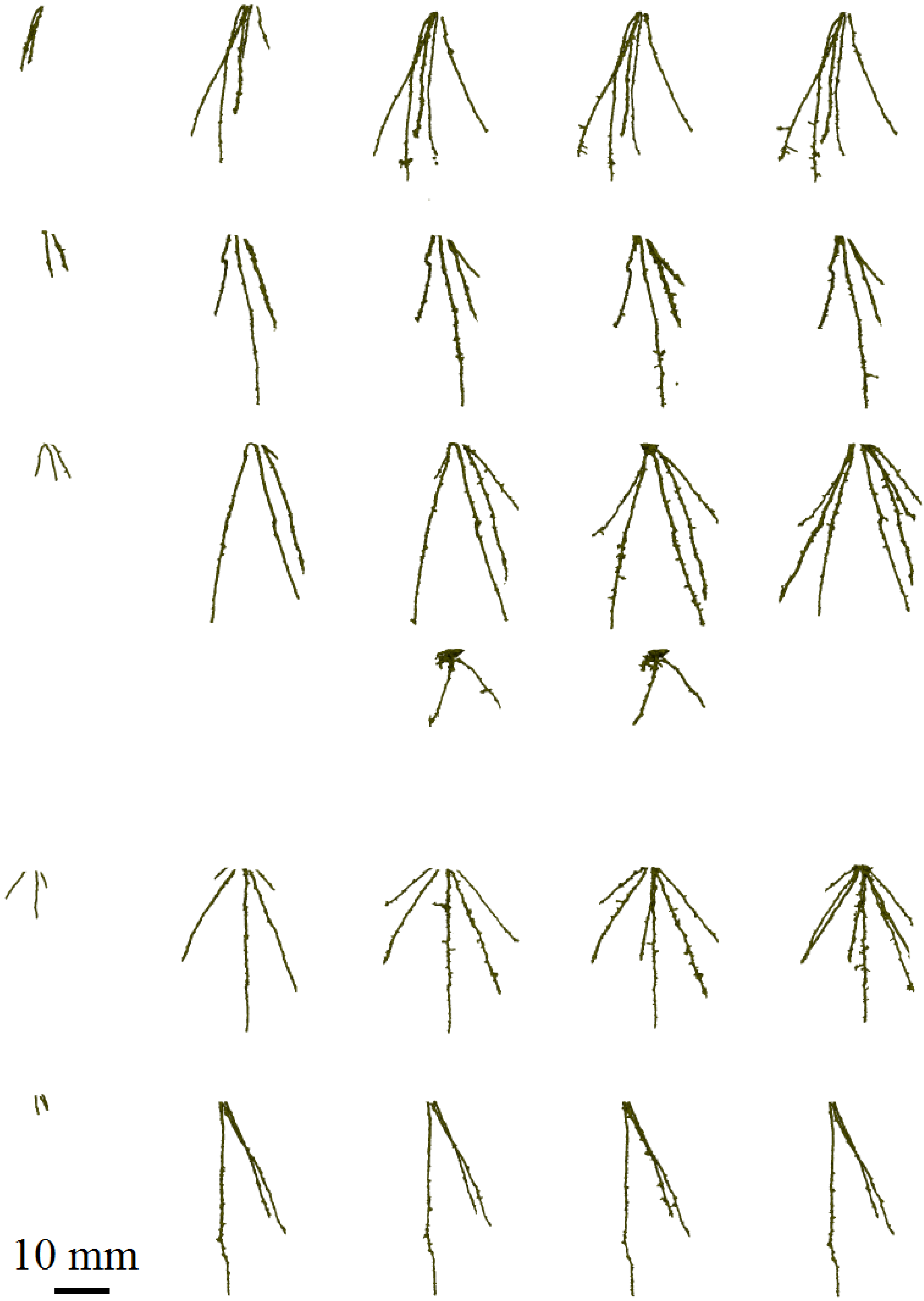

Figure 3: Root architectures for roots grown in clay loam soil. Each row is a different sample. Columns correspond to Day 2, Day 4, Day 6, Day 8, Day 12. Scale bar is 10 mm.

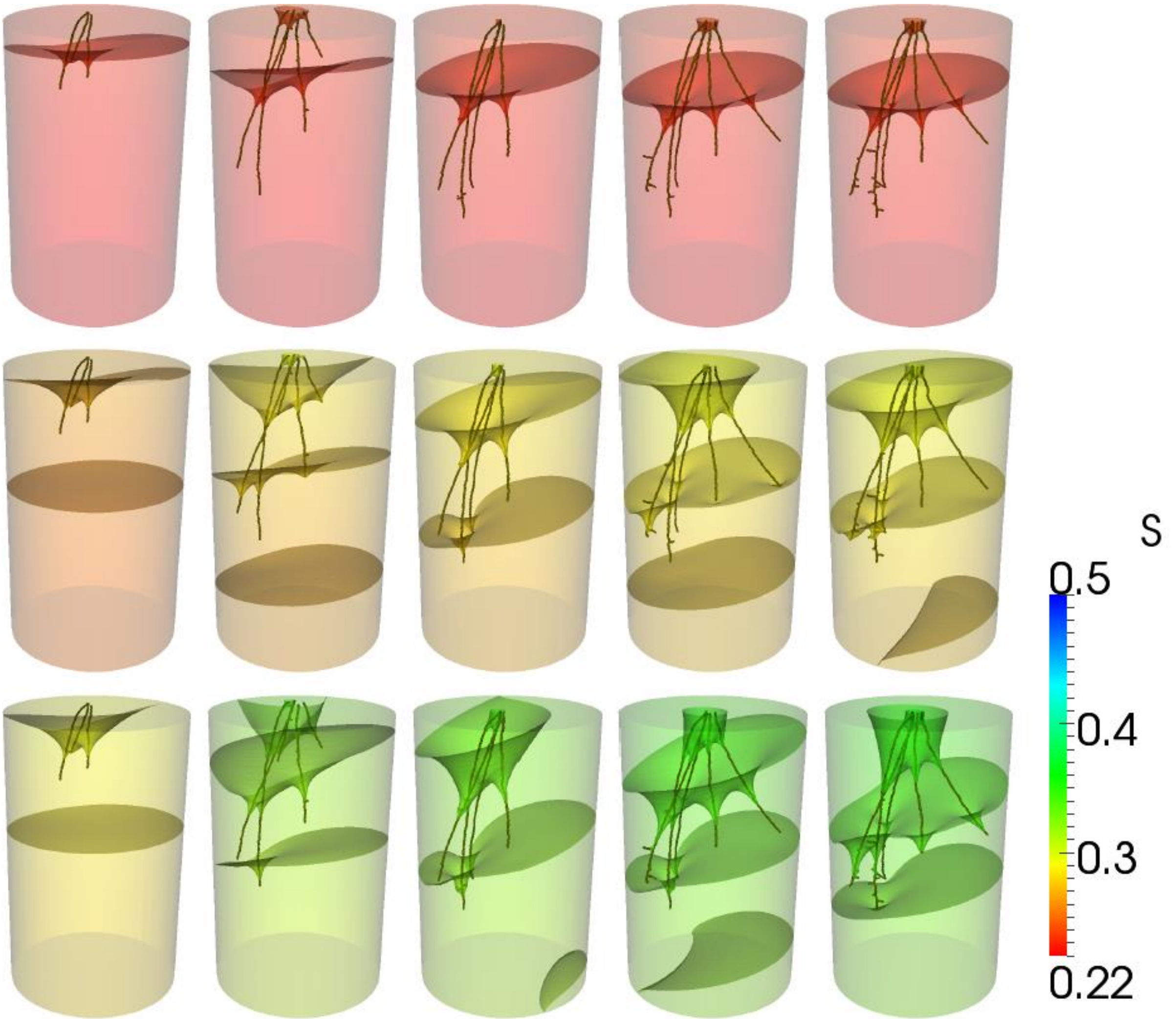

Figure 4: Water saturation (S) in loamy sand soil for a growing root system. Left to right shows the root system at 2, 4, 6, 8 and 12 days post transplanting. Images from top to bottom show half an hour of simulation, 6 hours of simulation and 12 hours of simulation. The images show the total geometry modelled, *i.e.*, the pot (50 mm diameter, 80 mm height) with the root architecture inside. The surfaces show regions of equal saturation with the colour representing the saturation at that point within the pot.

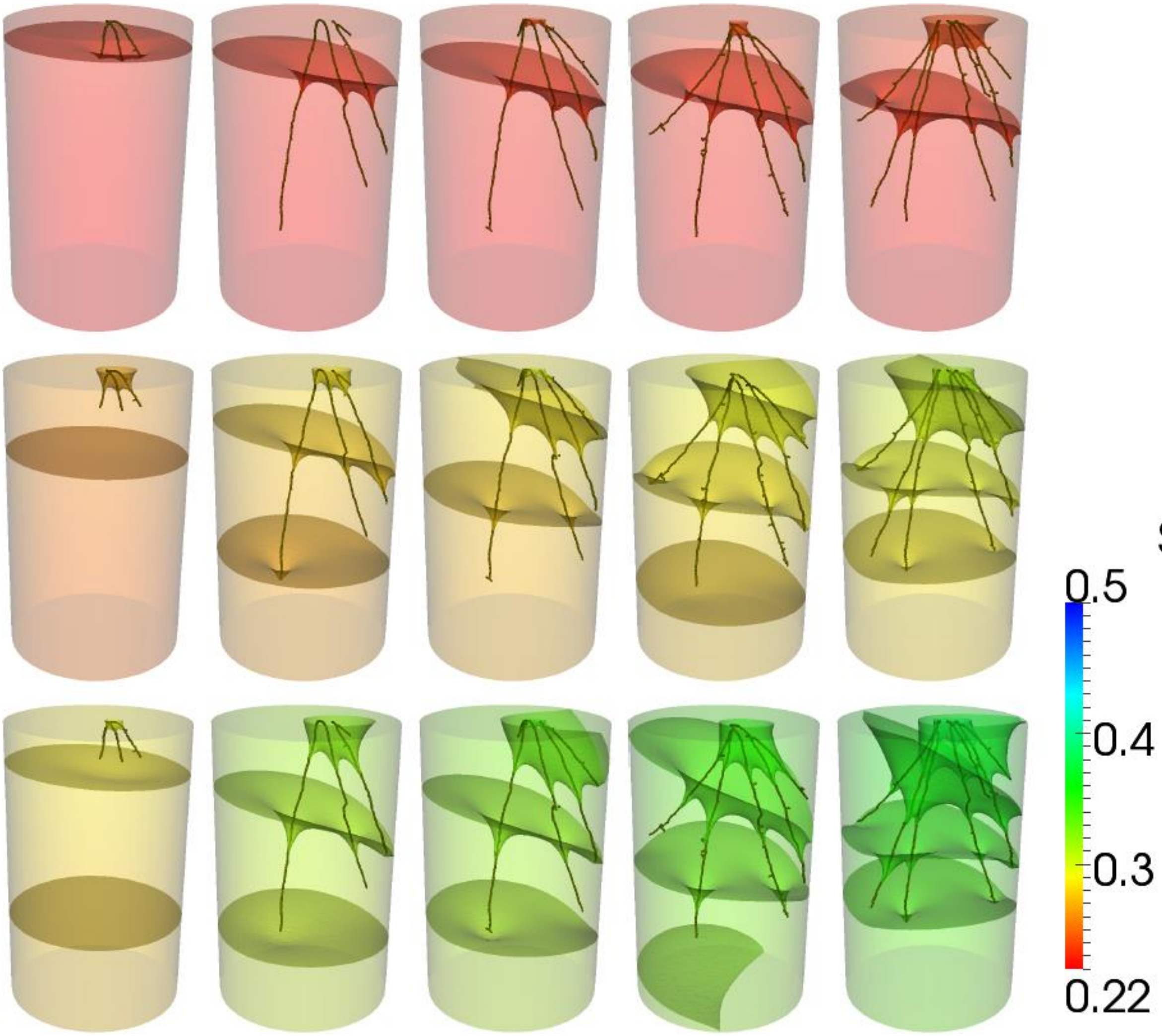

Figure 5: Water saturation (S) in a clay loam soil for a growing root system. Left to right shows the root system at 2, 4, 6, 8 and 12 days post transplanting. Images from top to bottom show half an hour of simulation, 6 hours of simulation and 12 hours of simulation. The images show the total geometry modelled, *i.e.*, the pot (50 mm diameter, 80 mm height) with the root architecture inside. The surfaces show regions of equal saturation with the colour representing the saturation at that point within the pot.

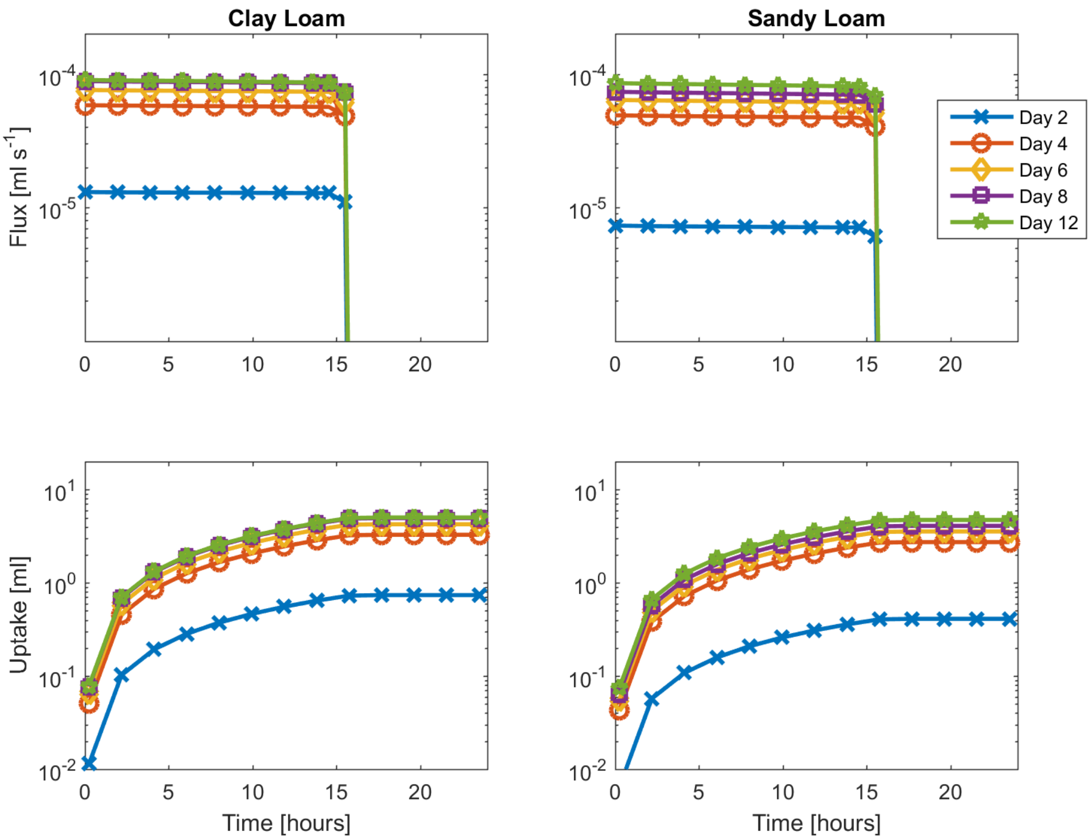

Figure 6 Water flux (top) and cumulative uptake (bottom) over a single day-night cycle for Clay loam (left) and loamy sand (right) soils. The data has been calculated using the image based modelling approach taking into account the full root geometry. Data is shown for 2, 4, 6, 8 and 12 days post transplantation. .

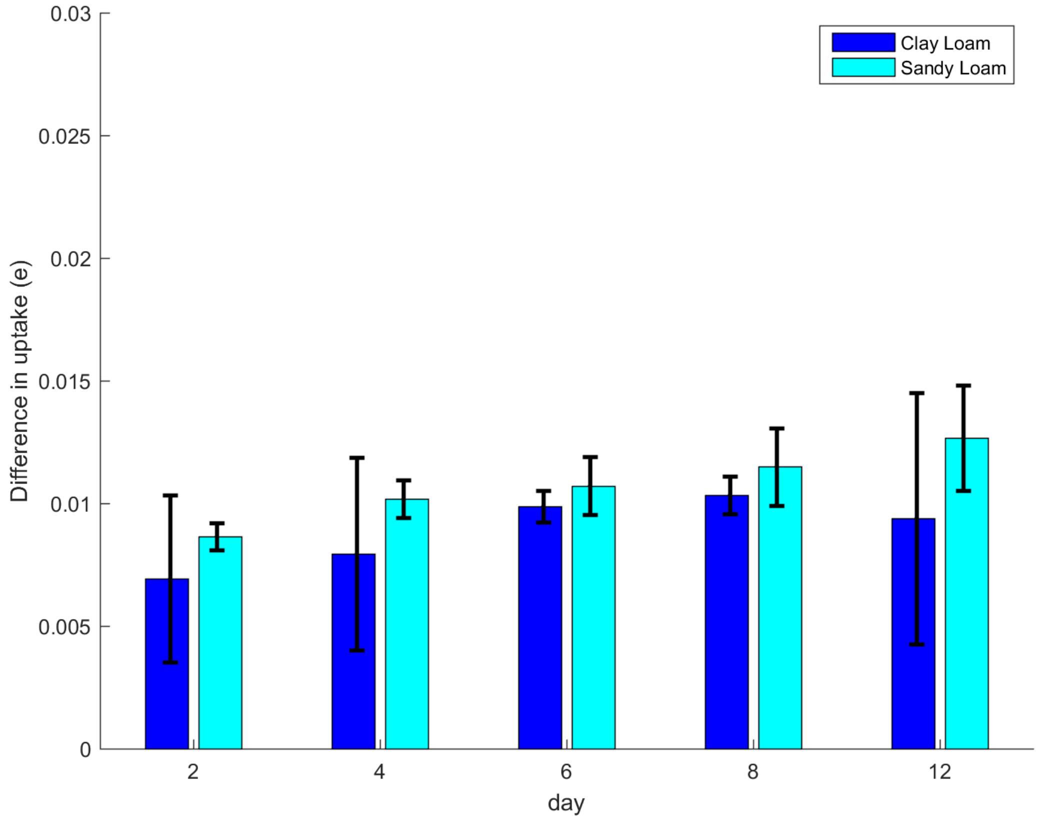

Figure 7 Relative difference in cumulative uptake (e), as defined by equation (11). The data shows the difference between the image based and averaged models for clay loam and loamy sand soils.

Table 1: Parameter values

Symbol	Value	Units	Description
K_s	Clay: 1.09×10^{-5} Sand: 2.46×10^{-5}	$\mathrm{m\ s^{-1}}$	Hydraulic conductivity (Daly et al., 2015)
ϕ	0.4		Soil porosity (Daly et al., 2015)
D_0	4.37×10^{-6}	$\mathrm{m^2\ s^{-1}}$	Soil water diffusivity (Van Genuchten, 1980)
m	Clay: 0.415 Sand: 0.397		Van Genuchten parameter (Daly et al., 2015)
ρ	10^3	$\mathrm{kg\ m^{-3}}$	Density of water
g	9.8	$\mathrm{m\ s^{-2}}$	Acceleration due to gravity
p_c	0.02	MPa	Characteristic suction pressure (Van Genuchten, 1980)
p_0	day: -1 night: 0	MPa	Root internal pressure (Passioura, 1983)
k_r	1.3×10^{-13}	$\mathrm{m\ s^{-1} Pa^{-1}}$	Radial conductivity (Jones et al., 1983)
k_z	2×10^{-16}	$\mathrm{m^4 s^{-1} Pa^{-1}}$	Axial conductivity (Payvandi et al., 2014; Percival, 1921)
L	60×10^{-3}	m	Typical root length (CT images)
a	390×10^{-6}	m	Root radius (CT images)